

# A comparison of different order hybrid finite difference-volume methods for solving the Serre equations in conservative law form

Jordan Pitt,<sup>1</sup>  
Christopher Zoppou,<sup>1</sup>  
Stephen G. Roberts,<sup>1</sup>

## ABSTRACT

**Keywords:** dispersive waves, conservation laws, Serre equation, finite volume method, finite difference method

## <sup>1</sup> INTRODUCTION

Free surface flows occur in many important applications such as; tsunamis, storm surges, tidal bores and riverine flooding. As these surfaces vary more rapidly the assumption of hydrostatic pressure in a fluid column breaks down and vertical acceleration inside the fluid becomes important. Therefore, the use of the shallow water wave equations is not fully justified as they enforce a hydrostatic pressure distribution. While numerical methods for the full Euler equations are not yet computationally efficient enough to deal with these problems over large domains to high accuracy. Thus the Serre equations have been developed to approximate the flow regime where the fluid is shallow  $\sigma \ll 1$  and fully non-linear  $\epsilon \sim 1$  (Lannes and Bonneton 2009).

The Serre equations were first derived by Serre (1953) for flat bottom topographies in one dimension. Su and Gardner (1969) obtained equations for any smooth bottom topographies in one dimension and Green and Naghdi (1976) did the same in two dimensions. These equations have been handled in many different ways (Mitsotakis et al. 2014; Bonneton et al. 2011; Antunes do Carmo et al. 1993; Chazel et al. 2011; Cienfuegos and Bonneton 2006; Cienfuegos and Bonneton 2007; Dutykh et al. 2011). This paper follows the decomposition of the Serre equations into conservative law form (Le Métayer et al. 2010; Li et al. 2014) and then follows the formulation of Le Métayer et al. (2010) and Zoppou (2014) to build a first-, second- and third-order scheme. The benefits of this method are its steep gradient handling capability and its ability to be extended to two dimensions. This paper investigates the steep gradient handling capability of the method while also examining how accurate a numerical scheme for the Serre equations should be

---

<sup>1</sup>Mathematical Sciences Institute, Australian National University, Canberra, ACT 0200, Australia, E-mail: Jordan.Pitt@anu.edu.au. The work undertaken by the first author was supported financially by an Australian National University Postgraduate Research Award.

23 to capture the important behaviour in one dimension; as a foundation for future work in  
 24 two dimensions.

25 Zoppou and Roberts (1996) demonstrated that first- and third-order schemes produce  
 26 diffusive errors smearing steep gradients. While second-order schemes produce dissipative  
 27 errors introducing non-physical oscillations around steep gradients. Because steep gradi-  
 28 ents arise naturally in fluid flows and the Serre equations produce dispersive waves around  
 29 them (El et al. 2006) it is important that these oscillations are not significantly polluted  
 30 by either diffusion or dissipation. Which was a problem apparent in the conflicting results  
 31 of El et al. (2006) and Le Métayer et al. (2010) with relation to the dam break problem  
 32 replicated in this paper.

### 33 SERRE EQUATIONS

34 The Serre equations can derived as an approximation to the full Euler equations by  
 35 depth integration similar to Su and Gardner (1969). They can also be seen as an asymp-  
 36 totic expansion to the Euler equations (Lannes and Bonneton 2009). The former is more  
 37 consistent with the perspective from which numerical methods will be developed in this  
 38 paper while the latter indicates the appropriate regions in which to use these equations as  
 39 a model for fluid flow.

40 The scenario under which the Serre approximation is made consists of a two dimen-  
 41 sional  $\mathbf{x} = (x, z)$  fluid over a bottom topography as in Figure 1, under the action of  
 42 gravity. The water depth is  $h(x, t)$  and  $z_b(x)$  is the bed elevation. The fluid is subject  
 43 to the pressure,  $p(\mathbf{x}, t)$  and gravitational acceleration,  $\mathbf{g} = (0, g)^T$  and has a velocity  
 44  $\mathbf{u} = (u(\mathbf{x}, t), w(\mathbf{x}, t))$ , where  $u(\mathbf{x}, t)$  is the velocity in the  $x$ -coordinate and  $w(\mathbf{x}, t)$  is the  
 45 velocity in the  $z$ -coordinate and  $t$  is time. Assuming that  $z_b(x)$  is constant the Serre equa-  
 46 tions read (Li et al. 2014; Zoppou 2014)

$$47 \quad \frac{\partial h}{\partial t} + \frac{\partial(\bar{u}h)}{\partial x} = 0 \quad (1a)$$

$$48 \quad \underbrace{\frac{\partial(\bar{u}h)}{\partial t} + \frac{\partial}{\partial x} \left( \bar{u}^2 h + \frac{gh^2}{2} \right)}_{\text{Shallow Water Wave Equations}} + \underbrace{\frac{\partial}{\partial x} \left( \frac{h^3}{3} \left[ \frac{\partial \bar{u}}{\partial x} \frac{\partial \bar{u}}{\partial x} - \bar{u} \frac{\partial^2 \bar{u}}{\partial x^2} - \frac{\partial^2 \bar{u}}{\partial x \partial t} \right] \right)}_{\text{Dispersion Terms}} = 0. \quad (1b)$$

49

50

51

52 Where  $\bar{u}$  is the average of  $u$  over the depth of water.

53 **Alternative Conservation Law Form of the Sere Equations**

54 In Le Métayer et al. (2010) and Zoppou (2014) it is demonstrated that the Serre equa-  
55 tions can be rearranged into a conservation law form, by introducing a new quantity

56

$$57 G = uh - h^2 \frac{\partial h}{\partial x} \frac{\partial u}{\partial x} - \frac{h^3}{3} \frac{\partial^2 u}{\partial x^2}. \quad (2)$$

58 Consequently, the equations can be rewritten as

59

$$60 \frac{\partial h}{\partial t} + \frac{\partial(uh)}{\partial x} = 0, \quad (3a)$$

61 and

62

$$63 \frac{\partial G}{\partial t} + \frac{\partial}{\partial x} \left( Gu + \frac{gh^2}{2} - \frac{2h^3}{3} \frac{\partial u}{\partial x} \frac{\partial u}{\partial x} \right) = 0 \quad (3b)$$

64 where the bar over  $u$  has been dropped to simplify the notation. Thus a hybrid method can  
65 be developed for the Serre equations that solves the elliptic problem (2) for  $u$  and then the  
66 conservation law (3) for  $h$  and  $G$  at some later time. Replicating the process of Le Métayer  
67 et al. (2010) and Zoppou (2014).

68 **NUMERICALLY SOLVING THE SERRE EQUATIONS WRITTEN IN  
69 CONSERVATION LAW FORM**

70 There are numerous ways a numerical method could be built to solve the Serre equa-  
71 tions in conservation law form, (3). For flows that contain steep gradients the finite volume  
72 method seems the most appropriate. A finite volume method to solve (3) updates the con-  
73 served quantities  $h$  and  $G$  over a single time step  $\Delta t$  for instance from time  $t^n$  to  $t^{n+1}$ . So  
74 that

75

$$76 \begin{bmatrix} h^{n+1} \\ G^{n+1} \end{bmatrix} = \mathcal{L}(h^n, G^n, u^n, \Delta t) \quad (4)$$

77 where  $\mathcal{L}$  is some numerical solver for (3). The complete solution also involves solving (2)  
78 for  $u$  given  $h$  and  $G$  denoted by

79

$$80 u = \mathcal{A}(h, G) \quad (5)$$

81

82 **METHOD FOR  $\mathcal{A}$**

83 In the above section a very general map of a typical update in these hybrid methods for  
84 the Serre equations and a discretisation in time were given. In this paper a fully discrete

85 system will be built hence a discretisation of space is also introduced; denoted by subscript  
 86  $i$  for example  $h_i^n \approx h(x_i, t^n)$ . Additionally, assuming that this discretisation in space has a  
 87 fixed resolution so that  $\forall i x_{i+1} - x_i = \Delta x$ ; allows for a simple finite difference approximation  
 88 to (2) as a suitable method for  $\mathcal{A}$  (Le Métayer et al. 2010; Zoppou 2014). Since the goal of  
 89 this paper is to develop and compare a range of different order methods for this problem  
 90 both a second- and fourth-order centred finite difference approximation to (2) were used.  
 91 By taking such approximations to the first- and second-order spatial derivatives the second-  
 92 and fourth-order analogues of (2) are given by

$$93 \quad G_i = u_i h_i - h_i^2 \left( \frac{h_{i+1} - h_{i-1}}{2\Delta x} \right) \left( \frac{u_{i+1} - u_{i-1}}{2\Delta x} \right) - \frac{h_i^3}{3} \left( \frac{u_{i+1} - 2u_i + u_{i-1}}{\Delta x^2} \right), \quad (6)$$

95 and

$$96 \quad G_i = u_i h_i - h_i^2 \left( \frac{-h_{i+2} + 8h_{i+1} - 8h_{i-1} + h_{i-2}}{12\Delta x} \right) \left( \frac{-u_{i+2} + 8u_{i+1} - 8u_{i-1} + u_{i-2}}{12\Delta x} \right) \\ 97 \quad - \frac{h_i^3}{3} \left( \frac{-u_{i+2} + 16u_{i+1} - 30u_i + 16u_{i-1} - u_{i-2}}{12\Delta x^2} \right). \quad (7)$$

98 Both of these can be rearranged into a matrix equation with the following form

$$99 \quad \begin{bmatrix} u_0 \\ \vdots \\ u_m \end{bmatrix} = A^{-1} \begin{bmatrix} G_0 \\ \vdots \\ G_m \end{bmatrix} =: \mathcal{A}(\mathbf{h}, \mathbf{G})$$

101 For a second-order approximation the matrix  $A$  is tri-diagonal while for a fourth-order  
 102 scheme it is penta-diagonal.

### 103 METHOD FOR $\mathcal{L}$

104 A finite volume method of sufficient order was developed to solve (3). Unlike finite  
 105 difference schemes which utilise nodal values of quantities, finite volume schemes use the  
 106 average of a value over a cell. To this end new notation is introduced by example, the  
 107 average water depth over a cell which spans  $[x_{i-\frac{1}{2}}, x_{i+\frac{1}{2}}]$  is

$$108 \quad \bar{h}_i = \frac{1}{\Delta x} \int_{x_{i-\frac{1}{2}}}^{x_{i+\frac{1}{2}}} h(x, t) dx$$

110 where  $x_{i\pm\frac{1}{2}} = x_i \pm \Delta x/2$ . Finite volume methods update the cell average values by the  
 111 following scheme

$$112 \quad \bar{U}_i^{n+1} = \bar{U}_i^n - \frac{\Delta t}{\Delta x} \left( F_{i+\frac{1}{2}}^n - F_{i-\frac{1}{2}}^n \right) \quad (8)$$

114 where  $\bar{U}_i^n = [\bar{h}_i^n \ \bar{G}_i^n]^T$  is an approximation of the vector of the conserved quantities aver-  
 115 aged over the cell at time  $t^n$ . While  $F_{i\pm 1/2}^n$  is an approximation of the average flux at  $x_{i\pm 1/2}$   
 116 over the time interval  $[t^n, t^{n+1}]$  which is given by solving the Riemann problem at the cell  
 117 boundaries.

118 *Local Riemann Problem*

119 Since  $\bar{U}_i^n$  is known what remains is to calculate the two time averaged fluxes  $F_{i\pm 1/2}$ . In  
 120 Kurganov et al. (2002) the time averaged inter-cell flux is approximated by

$$121 \quad F_{i+\frac{1}{2}} = \frac{a_{i+\frac{1}{2}}^+ f(q_{i+\frac{1}{2}}^-) - a_{i+\frac{1}{2}}^- f(q_{i+\frac{1}{2}}^+)}{a_{i+\frac{1}{2}}^+ - a_{i+\frac{1}{2}}^-} + \frac{a_{i+\frac{1}{2}}^+ a_{i+\frac{1}{2}}^-}{a_{i+\frac{1}{2}}^+ - a_{i+\frac{1}{2}}^-} [q_{i+\frac{1}{2}}^+ - q_{i+\frac{1}{2}}^-]. \quad (9)$$

122 where  $f$  is the instantaneous flux of the conservative law for the conserved quantity  $q$ .  
 While  $a_{i+1/2}^-$  and  $a_{i+1/2}^+$  are given by

$$a_{i+\frac{1}{2}}^- = \min \left[ \lambda_1 \left( q_{i+\frac{1}{2}}^- \right), \lambda_1 \left( q_{i+\frac{1}{2}}^+ \right), 0 \right], \quad (10a)$$

and

$$a_{i+\frac{1}{2}}^+ = \max \left[ \lambda_2 \left( q_{i+\frac{1}{2}}^- \right), \lambda_2 \left( q_{i+\frac{1}{2}}^+ \right), 0 \right] \quad (10b)$$

123 where  $\lambda_1$  and  $\lambda_2$  are estimates of the smallest and largest eigenvalues respectively of the  
 124 Jacobian. Which corresponds to the maximum and minimum phase speed  $v_p$  of the Serre  
 125 equations.

126 *Propagation Speeds of a Local Shock*

127 As demonstrated in Zoppou (2014)  $\lambda_1$  and  $\lambda_2$  are bounded by the phase speed of the  
 128 shallow water wave equations, so that

$$129 \quad \lambda_1 := u - \sqrt{gh} \leq v_p \leq u + \sqrt{gh} =: \lambda_2. \quad (11)$$

131 Thus  $a_{i+1/2}^-$  and  $a_{i+1/2}^+$  are fully determined.

132 *Reconstruction*

133 The quantities  $q_{i+1/2}^-$  and  $q_{i+1/2}^+$  are given by the two reconstructions at  $x_{i+1/2}$  one from  
 134 the cell to the left  $[x_{i-1/2}, x_{i+1/2}]$  and one from the cell to the right  $[x_{i+1/2}, x_{i+3/2}]$ , denoted  
 135 by the superscripts  $-$  and  $+$  respectively. The order of the polynomials used to reconstruct  
 136 the quantities inside the cells determines the order of the scheme in space. Polynomials  
 137 that are constant functions result in a first-order method (Godunov 1959). Similarly first-  
 138 and second-degree polynomials result in second- and third-order schemes respectively.

139 For a zero-degree polynomial the interpolant has the value  $\bar{q}_i$  at  $x_i$ , this is also the  
 140 case for linear interpolation functions. Thus in the zero-degree case the interpolants are  
 141 fully determined and monotonicity preserving. However, for higher-degree interpolants  
 142 there are a variety of ways to construct them. Not all of these are necessarily monotonicity  
 143 preserving which can result in the introduction of oscillations during the reconstruction  
 144 process. To suppress these non-physical oscillations in higher order schemes limiting  
 145 must be implemented. For the second-order scheme the minmod limiter was used as in  
 146 Kurganov et al. (2002). While for the third-order scheme the Koren limiter was used  
 147 (Koren 1993). This results in the following fitting scheme for second-order

$$148 \quad q_{i+\frac{1}{2}}^- = \bar{q}_i + a_i \frac{\Delta x}{2}, \quad (12a)$$

$$149$$

150 and

$$151 \quad q_{i+\frac{1}{2}}^+ = \bar{q}_{i+1} - a_{i+1} \frac{\Delta x}{2}, \quad (12b)$$

$$152$$

153 where

$$154 \quad a_i = \text{minmod} \left\{ \theta \frac{\bar{q}_{i+1} - \bar{q}_i}{\Delta x}, \frac{\bar{q}_{i+1} - \bar{q}_{i-1}}{2\Delta x}, \theta \frac{\bar{q}_i - \bar{q}_{i-1}}{\Delta x} \right\} \quad \text{for } \theta \in [1, 2]. \quad (12c)$$

$$155$$

156 For third-order

$$157 \quad q_{i+\frac{1}{2}}^- = \bar{q}_i + \frac{1}{2} \phi^-(r_i) (\bar{q}_i - \bar{q}_{i-1}), \quad (13a)$$

$$158$$

159 and

$$160 \quad q_{i+\frac{1}{2}}^+ = \bar{q}_i - \frac{1}{2} \phi^+(r_i) (\bar{q}_i - \bar{q}_{i-1}) \quad (13b)$$

$$161$$

162 where

$$163 \quad \phi^-(r_i) = \max \left[ 0, \min \left[ 2r_i, \frac{1+2r_i}{3}, 2 \right] \right], \quad (13c)$$

$$164$$

$$165$$

$$166 \quad \phi^+(r_i) = \max \left[ 0, \min \left[ 2r_i, \frac{2+r_i}{3}, 2 \right] \right], \quad (13d)$$

$$167$$

168 and

$$169 \quad r_i = \frac{\bar{q}_{i+1} - \bar{q}_i}{\bar{q}_i - \bar{q}_{i-1}}. \quad (13e)$$

$$170$$

171 Fully discrete approximations to flux function

172 For the water depth, the fully discrete approximation to  $f(h_{i+1/2}^\pm)$  is given by

$$173 \quad 174 \quad f\left(h_{i+\frac{1}{2}}^\pm\right) = u_{i+\frac{1}{2}}^\pm h_{i+\frac{1}{2}}^\pm \quad (14)$$

175 which is independent of the order of accuracy of the scheme. The flux  $f(G_{i+1/2}^\pm)$  is more  
176 complicated because of the derivative and is given by

$$177 \quad f\left(G_{i+\frac{1}{2}}^\pm\right) = u_{i+\frac{1}{2}}^\pm G_{i+\frac{1}{2}}^\pm + \frac{g\left(h_{i+\frac{1}{2}}^\pm\right)^2}{2} - \frac{2\left(h_{i+\frac{1}{2}}^\pm\right)^3}{3} \left[ \left( \frac{\partial u}{\partial x} \right)_{i+\frac{1}{2}}^\pm \right]^2. \quad (15)$$

179 There are multiple ways to approximate this derivative with different corresponding orders  
180 of accuracy. The first- and third-order approximations to the derivatives can be obtained  
181 by an upwind finite difference approximation. Additionally assuming that  $u$  is continuous  
182 a second-order approximation that has the correct order and is simpler to implement than  
183 its corresponding upwind finite difference approximation can be used. Thus the following  
184 approximations to the derivatives were obtained for first-order

$$185 \quad 186 \quad 187 \quad \left( \frac{\partial u}{\partial x} \right)_{i+\frac{1}{2}}^+ = \frac{u_{i+\frac{3}{2}}^+ - u_{i+\frac{1}{2}}^+}{\Delta x}, \quad (16a)$$

$$188 \quad 189 \quad \left( \frac{\partial u}{\partial x} \right)_{i+\frac{1}{2}}^- = \frac{u_{i+\frac{1}{2}}^- - u_{i-\frac{1}{2}}^-}{\Delta x}, \quad (16b)$$

190 second-order

$$191 \quad 192 \quad \left( \frac{\partial u}{\partial x} \right)_{i+\frac{1}{2}}^- = \left( \frac{\partial u}{\partial x} \right)_{i+\frac{1}{2}}^+ = \frac{u_{i+1} - u_i}{\Delta x}, \quad (17)$$

193 and third-order

$$194 \quad 195 \quad 196 \quad \left( \frac{\partial u}{\partial x} \right)_{i+\frac{1}{2}}^+ = \frac{-u_{i+\frac{3}{2}}^+ + 4u_{i+\frac{3}{2}}^+ - 3u_{i+\frac{1}{2}}^+}{\Delta x}, \quad (18a)$$

$$197 \quad 198 \quad 199 \quad \left( \frac{\partial u}{\partial x} \right)_{i+\frac{1}{2}}^- = \frac{3u_{i+\frac{1}{2}}^- - 4u_{i-\frac{1}{2}}^- + u_{i-\frac{3}{2}}^-}{\Delta x}. \quad (18b)$$

200 **Transforming between nodal values and cell averages**

201 The operator  $\mathcal{L}$  in (4) uses cell averages and values at the cell boundaries obtained from  
 202 them in the reconstruction process. While the operator  $\mathcal{A}$  in (5) uses nodal values at the  
 203 cell centres. Therefore, a transformation from the cell averages to the nodal values must  
 204 be made. For the first- and second-order schemes this distinction is trivial since  $\bar{q}_i = q_i$ .  
 205 However, for the third-order scheme this is a very important distinction and failure to  
 206 handle this correctly will result in a loss of accuracy. For this problem it is sufficient to use  
 207 a quadratic polynomial that gives the correct cell averages for the cell centred at  $x_i$  and its  
 208 two neighbours. Such a polynomial satisfies this equation

209

$$210 \quad q_i = \frac{-\bar{q}_{i+1} + 26\bar{q}_i - \bar{q}_{i-1}}{24}. \quad (19)$$

211 This results in a tri-diagonal matrix equation that transforms from cell averages to nodal  
 212 values denoted by  $\mathcal{M}$ . The inverse transformation  $\mathcal{M}^{-1}$  denotes the solution of the tri-  
 213 diagonal matrix equation given nodal values resulting in cell averages. This completes the  
 214 effort to solve the Serre equations (2) and (3) with the following process denoted by  $\mathcal{H}$

215

$$\mathcal{H}(\bar{\mathbf{U}}^n, \Delta t) = \begin{cases} \mathbf{U}^n &= \mathcal{M}^{-1}(\bar{\mathbf{U}}^n) \\ \mathbf{u}^n &= \mathcal{A}(\mathbf{U}^n) \\ \bar{\mathbf{u}}^n &= \mathcal{M}(\mathbf{u}^n) \\ \bar{\mathbf{U}}^{n+1} &= \mathcal{L}(\bar{\mathbf{U}}^n, \bar{\mathbf{u}}^n, \Delta t) \end{cases} \quad (20)$$

216

217 **Strong-Stability-Preserving Runge-Kutta Scheme**

218 The process above is first-order accurate in time. There are many methods to increase  
 219 the accuracy of a time step, this paper will follow the method of strong stability Runge-  
 220 Kutta steps as in Gottlieb et al. (2009) to construct fully second- and third-order schemes.  
 221 These are constructed by linear combinations of applications of  $\mathcal{H}$ . This leads to the  
 222 following processes for first-, second- and third-order time stepping schemes respectively

223

$$224 \quad \bar{\mathbf{U}}^{n+1} = \mathcal{H}(\bar{\mathbf{U}}^n, \Delta t), \quad (21)$$

225 and

226

$$227 \quad \bar{\mathbf{U}}^{(1)} = \mathcal{H}(\bar{\mathbf{U}}^n, \Delta t) \quad (22a)$$

228

229

$$230 \quad \bar{\mathbf{U}}^{(2)} = \mathcal{H}(\bar{\mathbf{U}}^{(1)}, \Delta t) \quad (22b)$$

231

232

$$233 \quad \bar{\mathbf{U}}^{n+1} = \frac{1}{2}(\bar{\mathbf{U}}^{(1)} + \bar{\mathbf{U}}^{(2)}), \quad (22c)$$

234 and

235  
236

$$\bar{\mathbf{U}}^{(1)} = \mathcal{H}(\bar{\mathbf{U}}^n, \Delta t) \quad (23a)$$

237

238  
239

$$\bar{\mathbf{U}}^{(2)} = \mathcal{H}(\bar{\mathbf{U}}^{(1)}, \Delta t) \quad (23b)$$

240

241  
242

$$\bar{\mathbf{U}}^{(3)} = \frac{3}{4}\bar{\mathbf{U}}^n + \frac{1}{4}\bar{\mathbf{U}}^{(2)}, \quad (23c)$$

243

244  
245

$$\bar{\mathbf{U}}^{(4)} = \mathcal{H}(\bar{\mathbf{U}}^{(3)}, \Delta t) \quad (23d)$$

246

247  
248

$$\bar{\mathbf{U}}^{n+1} = \frac{1}{3}\bar{\mathbf{U}}^n + \frac{2}{3}\bar{\mathbf{U}}^{(4)}. \quad (23e)$$

249

250 **Stability Constraint**

251 A necessary condition for stability of this scheme based on the finite volume method  
252 is the Courant-Friedrichs-Lowy condition (LeVeque 2002) which states that

253  
254

$$\Delta t < \frac{\Delta x}{2 \max(|\lambda_i|)} \forall i \quad (24)$$

255 where  $\lambda_i$  is the  $i$ th eigenvalue of the Jacobian of the flux vector.

256 **NUMERICAL SIMULATIONS**

257 The discussed methods will now be used to solve three different situations; the soliton  
258 which is an analytic solution of the Serre equations, one of the experiments conducted by  
259 Hammack and Segur (1978) and a dam break problem from El et al. (2006) and Le Métayer  
260 et al. (2010). The first two will be used to validate the models with the soliton used to  
261 establish the order of convergence of the models; while the second validates the behaviour  
262 of a steep gradient against experimental data. Lastly the dam break will be used to compare  
263 the results of this scheme with those of El et al. (2006) and Le Métayer et al. (2010).

264 **Soliton**

265 Currently cnoidal waves are the only family of analytic solutions to the Serre equations  
 266 (Carter and Cienfuegos 2011). Solitons are a particular instance of cnoidal waves and have  
 267 been used to verify the convergence rates of the proposed methods in this paper.

268 Solitons travel without deformation and for the Serre equations they have the following  
 269 form

$$270 \quad h(x, t) = a_0 + a_1 \operatorname{sech}^2(\kappa(x - ct)), \quad (25a)$$

272

$$273 \quad u(x, t) = c \left(1 - \frac{a_0}{h(x, t)}\right), \quad (25b)$$

274

275

$$276 \quad \kappa = \frac{\sqrt{3a_1}}{2a_0 \sqrt{a_0 + a_1}}, \quad (25c)$$

277 and

$$278 \quad c = \sqrt{g(a_0 + a_1)}, \quad (25d)$$

281 where,  $a_0$  and  $a_1$  are input parameters that determine the depth of the quiescent water and  
 282 the maximum height of the soliton above that respectively. In the simulation  $a_0 = 10\text{m}$ ,  
 283  $a_1 = 1\text{m}$  for  $x \in [-500\text{m}, 1500\text{m}]$  and  $t \in [0\text{s}, 100\text{s}]$ . With  $\Delta t = \lambda \Delta x$  where  $\lambda = 0.01$  and  
 284  $\theta = 1.2$  for the second-order reconstruction (12). The example results for  $\Delta x = 100/2^6\text{m}$   
 285 can be seen in Figure 3, while the relative error as measured by the L1-norm of the method  
 286 can be seen in Figure 2. For a vector  $\mathbf{q}$  and an approximation to it  $\mathbf{q}^*$  the relative error as  
 287 measured by the L1-norm is

$$288 \quad \text{L1}(\mathbf{q}, \mathbf{q}^*) = \frac{\sum_{i=1}^m |q_i - q_i^*|}{\sum_{i=1}^m |q_i|}. \quad (26)$$

290 Figure 2 demonstrates that the schemes all have the correct order of convergence in  
 291 both time and space as desired since  $\Delta t = \lambda \Delta x$ . However, this order of convergence is not  
 292 over all  $\Delta x$ . When  $\Delta x$  is large the actual problem is not discretised well since the cells are  
 293 too large to adequately resolve the problem; this causes the observed suboptimal rate of  
 294 convergence in Figure 2. When  $\Delta x$  is sufficiently small the numerical errors become small  
 295 enough that floating point errors are significant and this can also lead to suboptimal rates  
 296 of convergence as can be seen for the third-order method in Figure 2(c). Therefore, the  
 297 order of convergence for all methods is confirmed.

298     Figure 3 demonstrates the superiority of the second- and third-order methods compared  
299    to the first-order method. With the first-order methods significant attenuation of the wave  
300    due to its diffusive behaviour which creates a wider wave profile and some smaller trailing  
301    waves. However, the first-order method does produce the correct speed of the wave with a  
302    small phase error.

303     The second- and third-order methods resolve the soliton solution without noticeable  
304    deformation on a relatively coarse grid with less than 500 cells representing the actual  
305    wave. While Figure 2(b) and Figure 2(c) demonstrate that these schemes both have similar  
306    errors for the example soliton.

307     Due to higher complexity more computational effort is required for the third-order  
308    method than the first- and second-order methods. In particular on average a single time  
309    step for the first- and second-order methods took approximately 14% and 50% respectively  
310    of the time taken for a single time step of a third-order method. Even though these higher  
311    order methods take longer to do a single time step. Because the convergence rates are  
312    higher, coarser grids allow for an accurate resolution of the solution as demonstrated in  
313    Figure 2. Therefore, computational time can be recovered by decreasing resolution to get  
314    a method of similar accuracy that is quicker to run.

315     Since both the second- and third-order schemes have similar errors and resolve the  
316    problem well the extra effort in both building and running a third-order scheme as com-  
317    pared to a second-order one is not justified in this case. While the effort required to go  
318    from a first-order to a second-order scheme is justified since attaining a similar accuracy  
319    between them requires a restrictively small  $\Delta x$  for a first-order method.

### 320    **Segur Laboratory Experiment**

321     Hammack and Segur (1978) conducted an experiment that produced rectangular waves  
322    with the stroke of a 0.61m long piston flush with the wall of a wave tank 31.6m long. The  
323    water height was recorded at 0m, 5m, 10m, 15m and 20m from the edge of the piston  
324    furthest from the wall over time. The quiescent water height  $h_1$  was 0.1m while the stroke  
325    of the piston caused a depression with water suddenly  $h_0 = 0.095\text{m}$  deep. To run this as  
326    a numerical simulation the reflected problem was used. This reflects the initial conditions  
327    of the simulation around the origin and doubles  $h_1 - h_0$  by changing  $h_0$ . Thus the domain  
328    was chosen to be from  $-60\text{m}$  to  $60\text{m}$  and the simulation was run for 50s with  $\Delta x = 0.01\text{m}$ ,  
329     $\lambda = 0.2/\sqrt{gh_1}\text{m/s}$  and  $\theta = 1.2$ . The results of this simulation are displayed in figures 4 - 6.

330     In this experiment for the positive side of the axis the initial depression causes a right  
331    going rarefaction fan and a left going shock. The shocks from both sides then reflect in  
332    the middle and so the shock and the rarefaction fan will travel in the same direction. The  
333    leading wave in all the related figures is the rarefaction fan while the trailing dispersive  
334    waves are the result of the reflected shock.

335     From all the related figures it can be seen that all models show good agreement between

336 the arrival of the first wave and the period of all the waves. While Figure 4 shows the first-  
 337 order model is too diffusive and thus under estimates the heights of the dispersive waves.  
 338 While the second- and third-order methods over estimate them. This discrepancy can be  
 339 explained by the Serre equations not taking into account viscous effects that may diffuse  
 340 the dispersive waves and so the Serre equations are actually producing an upper bound  
 341 on the wave heights for fluids with viscosity. Although even without these effects these  
 342 numerical methods show good agreement with the experimental data thus validating them  
 343 to correctly handle rapidly-varying fluids. In addition, it demonstrates that the oscillations  
 344 observed by the produced numerical solutions of the Serre equation around steep gradients  
 345 as in the dam break problem below, are physical and not numerical. This is of particular  
 346 importance to the second-order method which is known (Zoppou and Roberts 1996) to  
 347 produce non-physical oscillations in the solution.

### 348 Dam Break

349 The dam break problem can be defined as such

$$350 \quad h(x, 0) = \begin{cases} 1.8 & x < 500 \\ 1.0 & x \geq 500 \end{cases}, \quad (27)$$

$$353 \quad u(x, 0) = 0.0m/s. \quad (28)$$

355 With  $x \in [0m, 1000m]$  for  $t \in [0s, 30m]$ . Where  $\lambda = 0.01m/s$  and  $\theta = 1.2$ . This cor-  
 356 responds to sub-critical flow and was a situation demonstrated in El et al. (2006) and  
 357 Le Métayer et al. (2010). An example was plotted for  $\Delta x = 100/2^{10}m$  for all the methods  
 358 in Figure 8. To determine if the oscillations that occur in the solution indeed converge to  
 359 some limit as  $\Delta x \rightarrow 0$  multiple  $\Delta x$  values were run and then the amount of variation in  
 360 the solution measured. This will measure how oscillatory the solution was and be used  
 361 to determine the growth of the oscillations. A common way to measure this is the total  
 362 variation  $TV$  (LeVeque 2002) which for  $q$  is given by

$$363 \quad TV(q) = \sum_{\forall i \geq 1} |q_i - q_{i-1}|. \quad (29)$$

365 If the solution does indeed converge then the  $TV$  must at some point plateau so that more  
 366 oscillations cannot be introduced and those that are already present are bounded.

367 This was indeed the findings of the experiments as can be seen by Figure 7. As for  
 368 larger  $\Delta x$  the  $TV$  increased as  $\Delta x$  decreased because the models resolved more dispersive  
 369 waves. While as  $\Delta x$  decreased further the  $TV$  plateaued and so the size and number of  
 370 oscillations was bounded. Therefore, the scheme has not become unstable which supports

371 that this formulation handles steep gradients and the resultant dispersive waves well. There  
372 is also good agreement between the second- and third-order schemes under this measure.

373 These solutions compare very well to the findings in (El et al. 2006) with both the  
374 second- and third-order schemes resolving the oscillations around the 'contact discontinuity'(El et al. 2006)  
375 between the rarefaction fan and the shock. In Le Métayer et al. (2010)  
376 it was reported that for their first-order scheme such oscillatory behaviour was not seen.  
377 However, for the first order scheme proposed in this paper when  $\Delta x = 100/2^{16}$  it was  
378 resolved as in Figure 9. Thus this scheme validates the findings in El et al. (2006).

379 There is also a good agreement between the second- and third-order simulations of the  
380 dam break problem as can be seen in Figure 8. Although more oscillations are resolved by  
381 the third-order scheme over the second-order scheme, there is no significant change in the  
382 resolved behaviour of this problem between the two. As noted in the introduction second-  
383 order errors are dissipative, since the third-order scheme resolved the same oscillations it  
384 was demonstrated that none of the dissipative errors significantly polluted the wave train  
385 and so the second-order scheme sufficiently resolved the problem.

## 386 CONCLUSIONS

387 A first-, second- and third-order hybrid finite difference-volume scheme were devel-  
388 oped to solve the Serre equations written in conservative law form. The schemes were  
389 then tested and validated. Firstly the order of the schemes were all verified, secondly  
390 the schemes steep gradient handling capability was validated by comparison with experi-  
391 mental data. Thirdly the behaviour of the solutions matched previous findings in El et al.  
392 (2006). Thus it can be concluded that these methods are all valid and they properly handle  
393 shocks. It was also demonstrated that for these equations although second-order is not as  
394 accurate as third-order it still provides a satisfactory method for reasonable  $\Delta x$  unlike the  
395 first-order method which due to strong diffusion requires computationally restrictive  $\Delta x$  to  
396 produce satisfactory accuracy.

## 397 ACKNOWLEDGEMENTS

## 398 REFERENCES

- 399 Antunes do Carmo, A., Seabra-Santos, F. J., and Almeida, A. B. (1993). "Numerical solu-  
400 tion of the generalized serre equations with the maccormack finite-difference scheme."  
401 *International Journal for Numerical Methods in Fluids*, 16(8), 725–738.
- 402 Bonneton, P., Chazel, F., Lannes, D., Marche, F., and Tissier, M. (2011). "A splitting  
403 approach for the fully nonlinear and weakly dispersive green-naghdi model." *Journal of  
404 Computational Physics*, 230(4), 1479–1498.
- 405 Carter, J. D. and Cienfuegos, R. (2011). "Solitary and cnoidal wave solutions of the serre  
406 equations and their stability." *European Journal of Mechanics B/Fluids*, 30(3), 259–268.

- 407 Chazel, F., Lannes, D., and Marche, F. (2011). "Numerical simulation of strongly nonlinear  
 408 and dispersive waves using a green-naghdi model." *Journal of Scientific Computing*,  
 409 48(1-3), 105–116.
- 410 Cienfuegos, R. and Barthélemy, E. and Bonneton, P. (2006). "A fourth-order compact finite  
 411 volume scheme for fully nonlinear and weakly dispersive boussinesq-type equations.  
 412 part i: model development and analysis." *International Journal for Numerical Methods  
 413 in Fluids*, 51, 1217–1253.
- 414 Cienfuegos, R. and Barthélemy, E. and Bonneton, P. (2007). "A fourth-order compact fi-  
 415 nite volume scheme for fully nonlinear and weakly dispersive boussinesq-type equa-  
 416 tions. part ii: Boundary conditions and validation." *International Journal for Numerical  
 417 Methods in Fluids*, 53, 1423–1455.
- 418 Dutykh, D., Clamond, D., Milewski, P., and Mitsotakis, D. (2011). "Finite volume and  
 419 pseudo-spectral schemes for the fully nonlinear 'irrotational' serre equations." *Arxiv*,  
 420 24(5), 0 – 25.
- 421 El, G., Grimshaw, R. H. J., and Smyth, N. F. (2006). "Unsteady undular bores in fully  
 422 nonlinear shallow-water theory." *Physics of Fluids*, 18(027104).
- 423 Godunov, S. K. (1959). "A difference method for numerical calculation of discontinuous  
 424 solutions of the equations of hydrodynamics." *Matematicheskii Sbornik*, 89(3), 271–  
 425 306.
- 426 Gottlieb, S., Ketcheson, D. I., and Shu, C. W. (2009). "High order strong stability preserv-  
 427 ing time discretizations." *Journal of Scientific Computing*, 38(3), 251–289.
- 428 Green, A. E. and Naghdi, P. M. (1976). "A derivation of equations for wave propagation  
 429 in water of variable depth." *Journal of Fluid Mechanics*, 78(2), 237–246.
- 430 Hammack, J. L. and Segur, H. (1978). "The korteweg-de vries equation and water waves.  
 431 part 3. oscillatory waves." *Journal of Fluid Mechanics*, 84(2), 337–358.
- 432 Koren, B. (1993). "A robust upwind discretization method for advection, diffusion and  
 433 source terms." *Notes on Numerical Fluid Mechanics*, Vol. 45, Centrum voor Wiskunde  
 434 en Informatica, Amsterdam.
- 435 Kurganov, A., Noelle, S., and Petrova, G. (2002). "Semidiscrete central-upwind schemes  
 436 for hyperbolic conservation laws and hamilton-jacobi equations." *Journal of Scientific  
 437 Computing, Society for Industrial and Applied Mathematics*, 23(3), 707–740.
- 438 Lannes, D. and Bonneton, P. (2009)." *Physics of Fluids*, 21(1), 16601–16610.
- 439 Le Métayer, O., Gavrilyuk, S., and Hank, S. (2010). "A numerical scheme for the green-  
 440 naghdi model." *Journal of Computational Physics*, 229(6), 2034–2045.
- 441 LeVeque, R. (2002). *Finite Volume Methods for Hyperbolic Problems*, Vol. 54 of *Cam-  
 442 bridge Texts in Applied Mathematics*. Cambridge University Press.
- 443 Li, M., Guyenne, P., Li, F., and Xu, L. (2014). "High order well-balanced cdg-fe methods  
 444 for shallow water waves by a green-naghdi model." *Journal of Computational Physics*,

- 445      257, 169–192.
- 446      Mitsotakis, D., Ilan, B., and Dutykh, D. (2014). “On the galerkin/finite-element method  
447      for the serre equations.” *Journal of Scientific Computing*, 61(1), 166–195.
- 448      Serre, F. (1953). “Contribution à l’étude des écoulements permanents et variables dans les  
449      canaux.” *La Houille Blanche*, 6, 830–872.
- 450      Su, C. H. and Gardner, C. S. (1969). “Korteweg-de vries equation and generalisations. iii.  
451      derivation of the korteweg-de vries equation and burgers equation.” *Journal of Mathematical Physics*, 10(3), 536–539.
- 453      Zoppou, C. (2014). “Numerical solution of the one-dimensional and cylindrical serre equa-  
454      tions for rapidly varying free surface flows.” Ph.D. thesis, Australian National University,  
455      Australian National University.
- 456      Zoppou, C. and Roberts, S. (1996). “Behaviour of finite difference schemes for advection  
457      diffusion equations.” *Technical Report Mathematics Research Report No.MRR 062-96*.

458      **NOTATION**

459      *The following symbols are used in this paper:*

- $\mathcal{A}$  = Scheme to solve (2)
- $a$  = characteristic order of free surface amplitude;
- $B$  = characteristic order of bottom topography variation;
- $g$  = acceleration due to gravity on earth ( $m/s^2$ )
- $\mathcal{H}$  = Scheme to solve (1) over a single time step
- $H$  = characteristic water depth;
- $h$  = water depth (m);
- $\mathcal{L}$  = Scheme to solve (3)
- $L$  = characteristic horizontal scale;
- $p$  = pressure ( $N/m^2$ );
- $u$  = fluid particle velocity  $x$ -direction ( $m/s$ );
- $w$  = fluid particle velocity  $z$ -direction ( $m/s$ );
- $\epsilon$  = nonlinearity parameter  $a/H$  ;
- $\xi$  = water depth from free surface (m) ;
- $\Delta x$  = fixed resolution of  $x$  ;
- $\Delta t$  = resolution of  $t$  ;
- $\lambda$  = eigenvalues of the Jacobian ;
- $\sigma$  = shallowness parameter  $H^2/L^2$ .

460      **SUBSCRIPTS**

461       $i$  = space discretisation.

<sup>462</sup> **SUPERSCRIPTS**

<sup>463</sup>  $n$  = time discretisation.

<sup>464</sup> **ACCENTS**

<sup>465</sup>  $\bar{q}$  = quantity  $q$  averaged over the depth of water

$\bar{q}$  = quantity  $q$  averaged over a  $\Delta x$  length interval of space [only make sense given a  $x$  position to cer

466 **List of Figures**

467 1	The notation used for one-dimensional flow governed by the Serre equation.	18
468 2	Convergence of relative error using L1 norm for analytic soliton solution for both $h$ (○) and $u$ (◇) for the; (a) first-, (b) second- and (c) third-order schemes. . . . .	19
471 3	The first-, second- and third-order simulation of a soliton with $\Delta x = 100/2^6 m$ (○) plotted against the analytic solution of (6) (—) with black for $t = 0$ s and blue for $t = 100$ s. . . . .	20
474 4	Simulation of the rectangular wave experiment using the for first-order scheme at $x/h_0$ : (a) 0, (b) 50, (c) 100, (d) 150 and (e) 200 . . . . .	21
476 5	Simulation of the rectangular wave experiment using the for second-order scheme at $x/h_0$ : (a) 0, (b) 50, (c) 100, (d) 150 and (e) 200 . . . . .	22
478 6	Simulation of the rectangular wave experiment using the for third-order scheme at $x/h_0$ : (a) 0, (b) 50, (c) 100, (d) 150 and (e) 200 . . . . .	23
480 7	The change in total variation (TV) over $\Delta x$ for; (○) first- , (□) second-, and (◇) third-order schemes. . . . .	24
482 8	Solution of the dam break problem using the (a) first-, (b) second- and (c) third-order schemes. . . . .	25
484 9	Solution of the dam break problem using first-order scheme with $\Delta x =$ $100/2^{16} m$ . . . . .	26

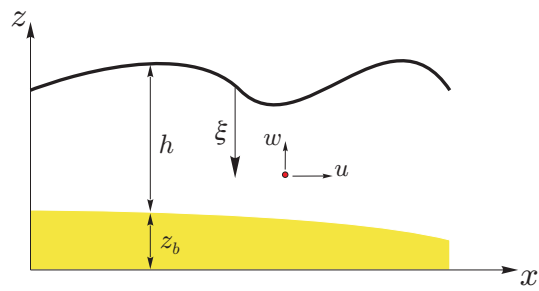


FIG. 1: The notation used for one-dimensional flow governed by the Serre equation.

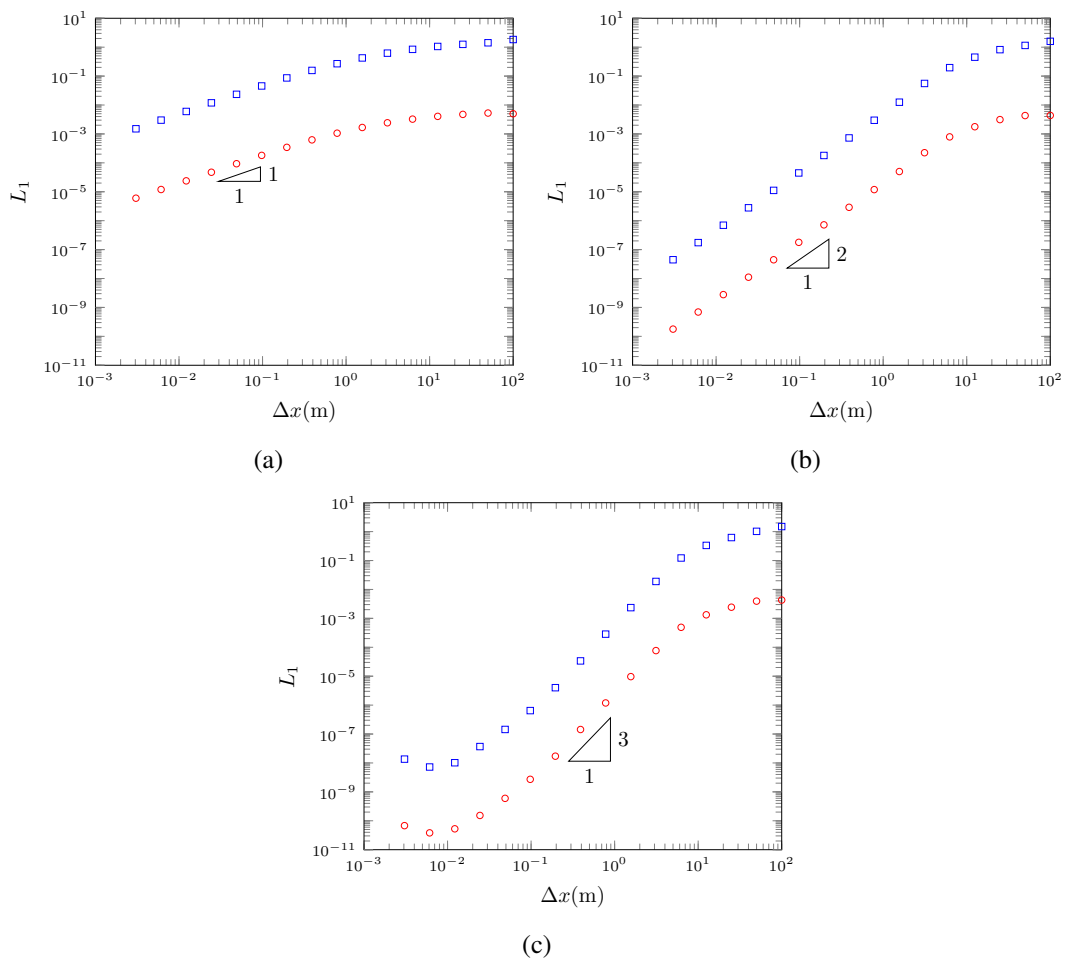


FIG. 2: Convergence of relative error using L1 norm for analytic soliton solution for both  $h$  ( $\circ$ ) and  $u$  ( $\diamond$ ) for the; (a) first-, (b) second- and (c) third-order schemes.

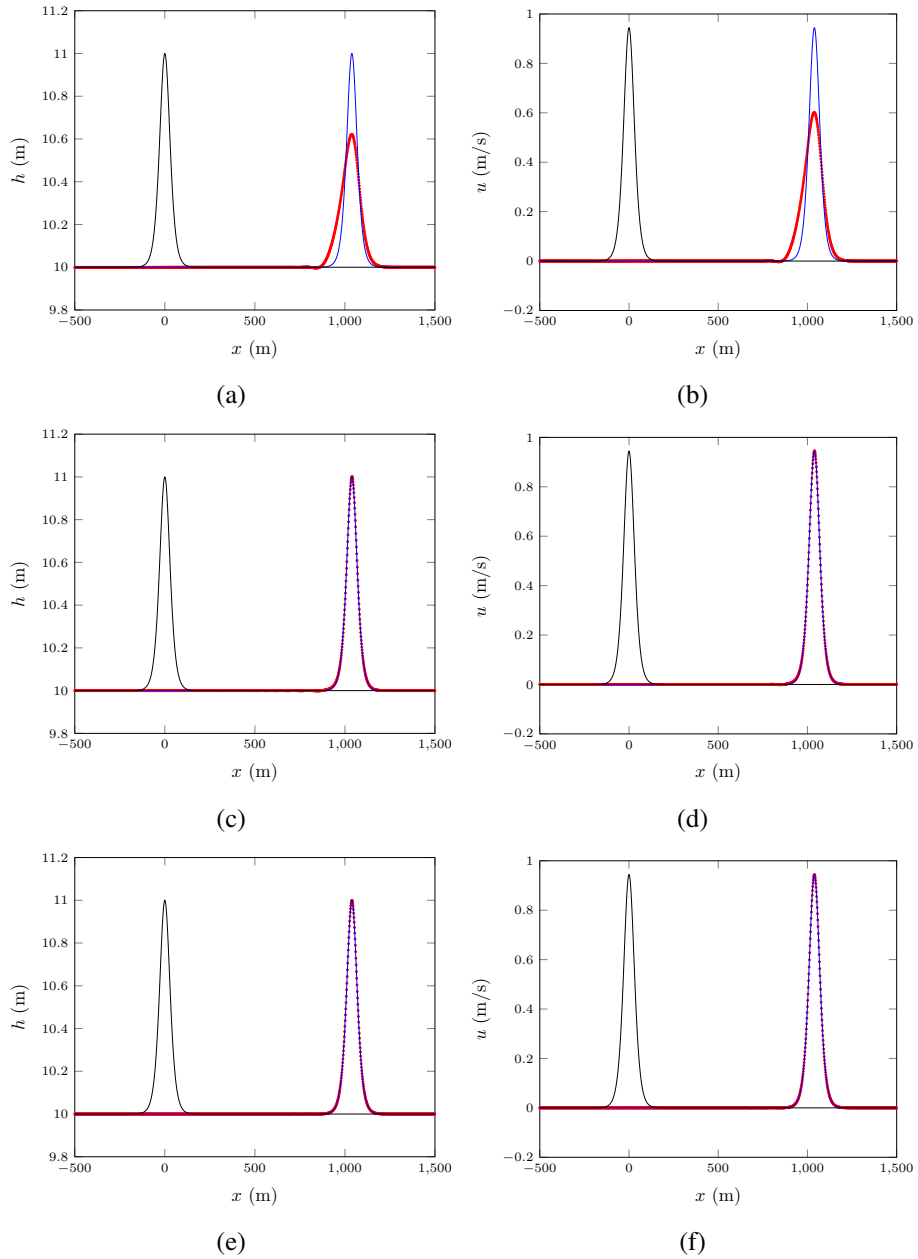


FIG. 3: The first-, second- and third-order simulation of a soliton with  $\Delta x = 100/2^6$ m (○) plotted against the analytic solution of (6) (—) with black for  $t = 0$ s and blue for  $t = 100$ s.

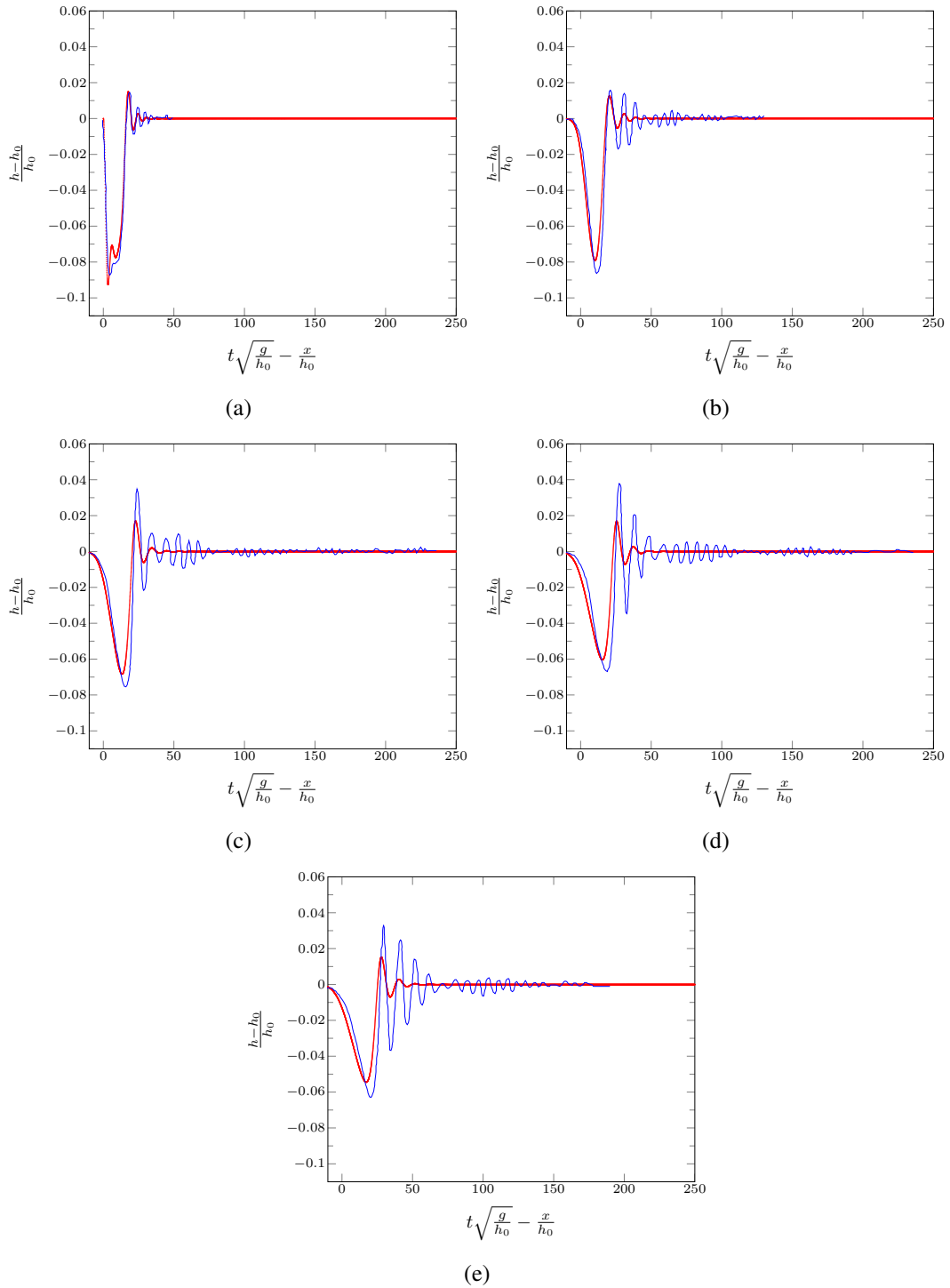


FIG. 4: Simulation of the rectangular wave experiment using the for first-order scheme at  $x/h_0$ : (a) 0, (b) 50, (c) 100, (d) 150 and (e) 200

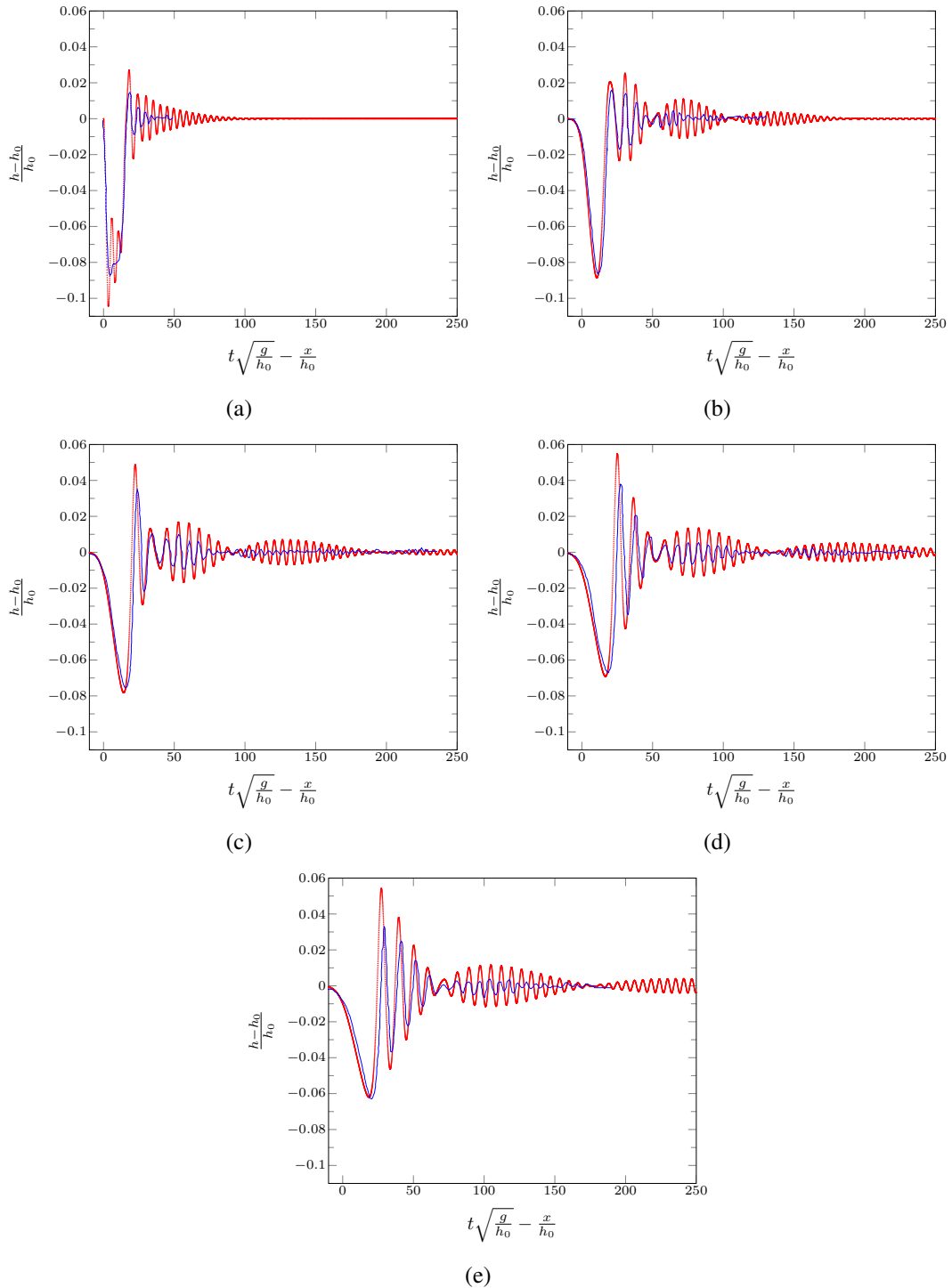


FIG. 5: Simulation of the rectangular wave experiment using the for second-order scheme at  $x/h_0$  : (a) 0, (b) 50, (c) 100, (d) 150 and (e) 200

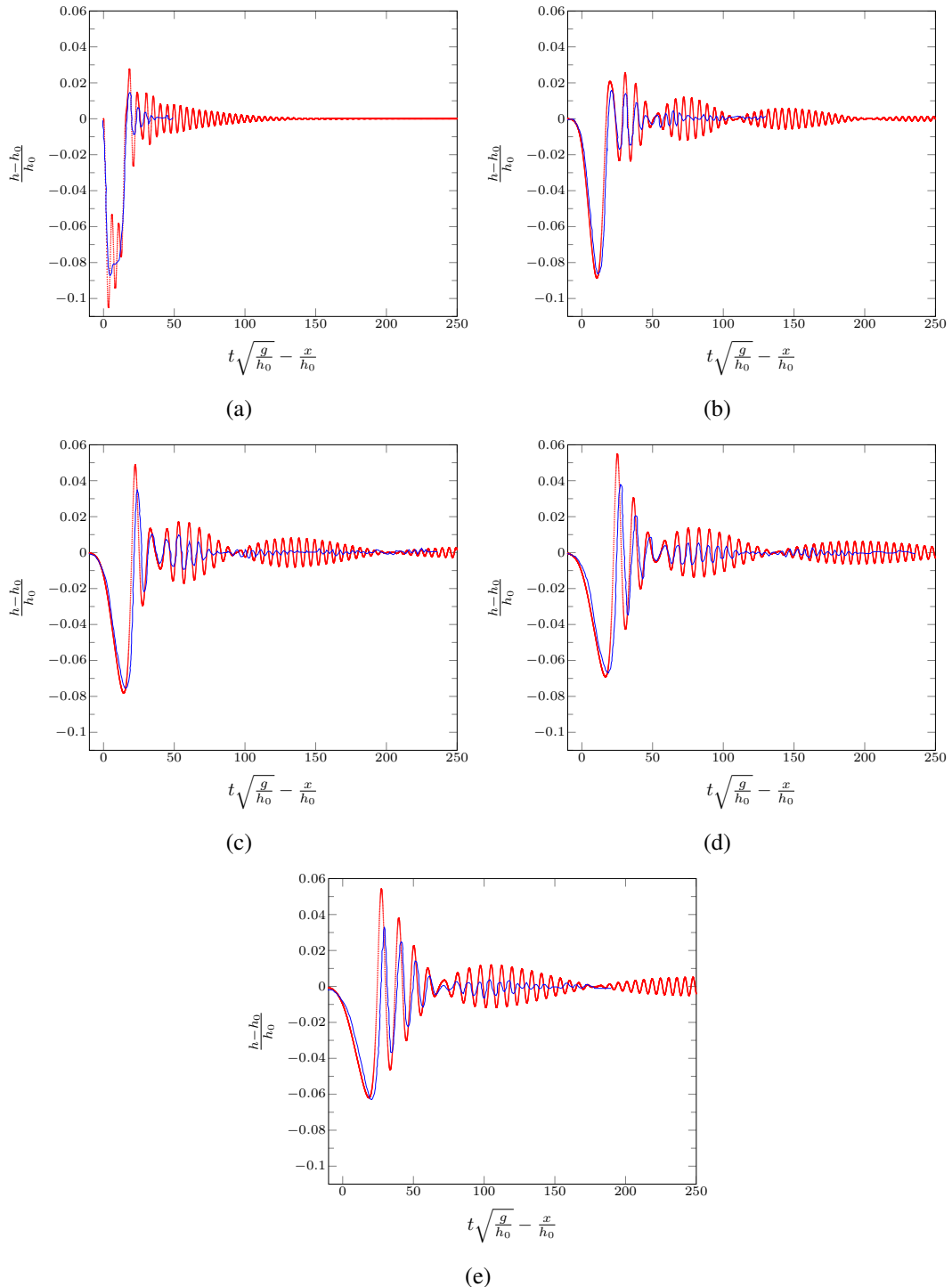


FIG. 6: Simulation of the rectangular wave experiment using the for third-order scheme at  $x/h_0$ : (a) 0, (b) 50, (c) 100, (d) 150 and (e) 200

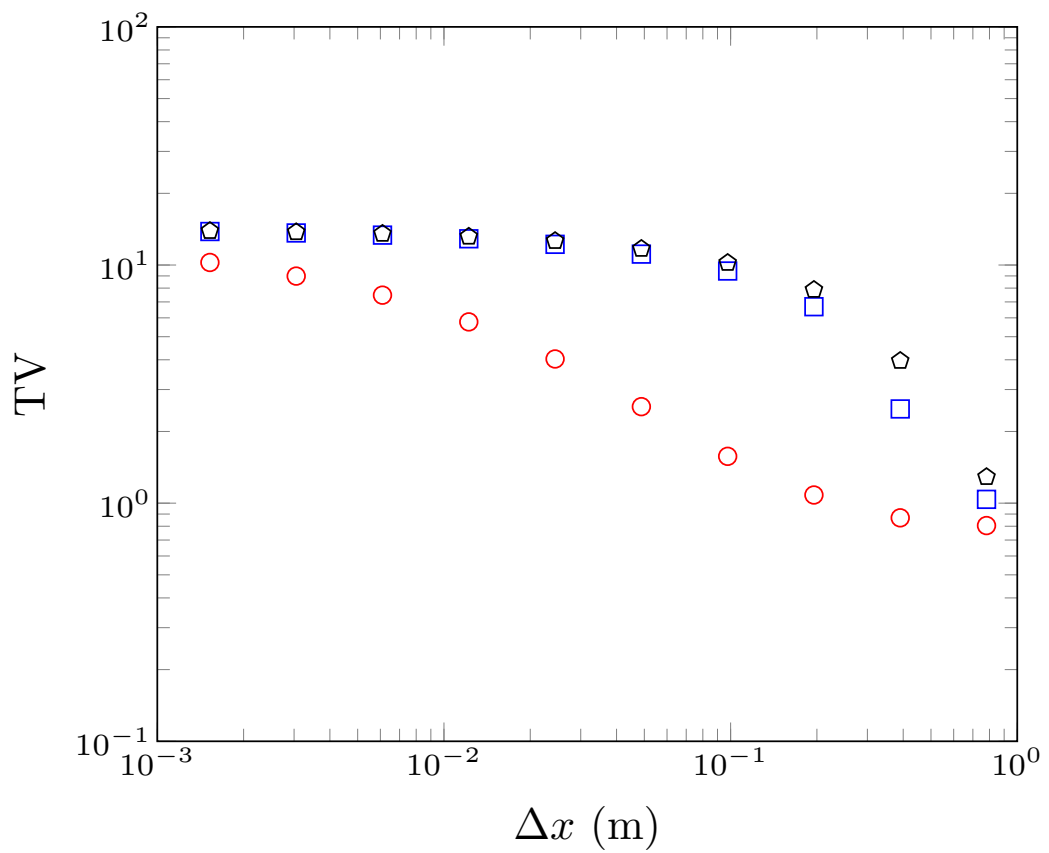


FIG. 7: The change in total variation (TV) over  $\Delta x$  for; (○) first-, (□) second-, and (◇) third-order schemes.

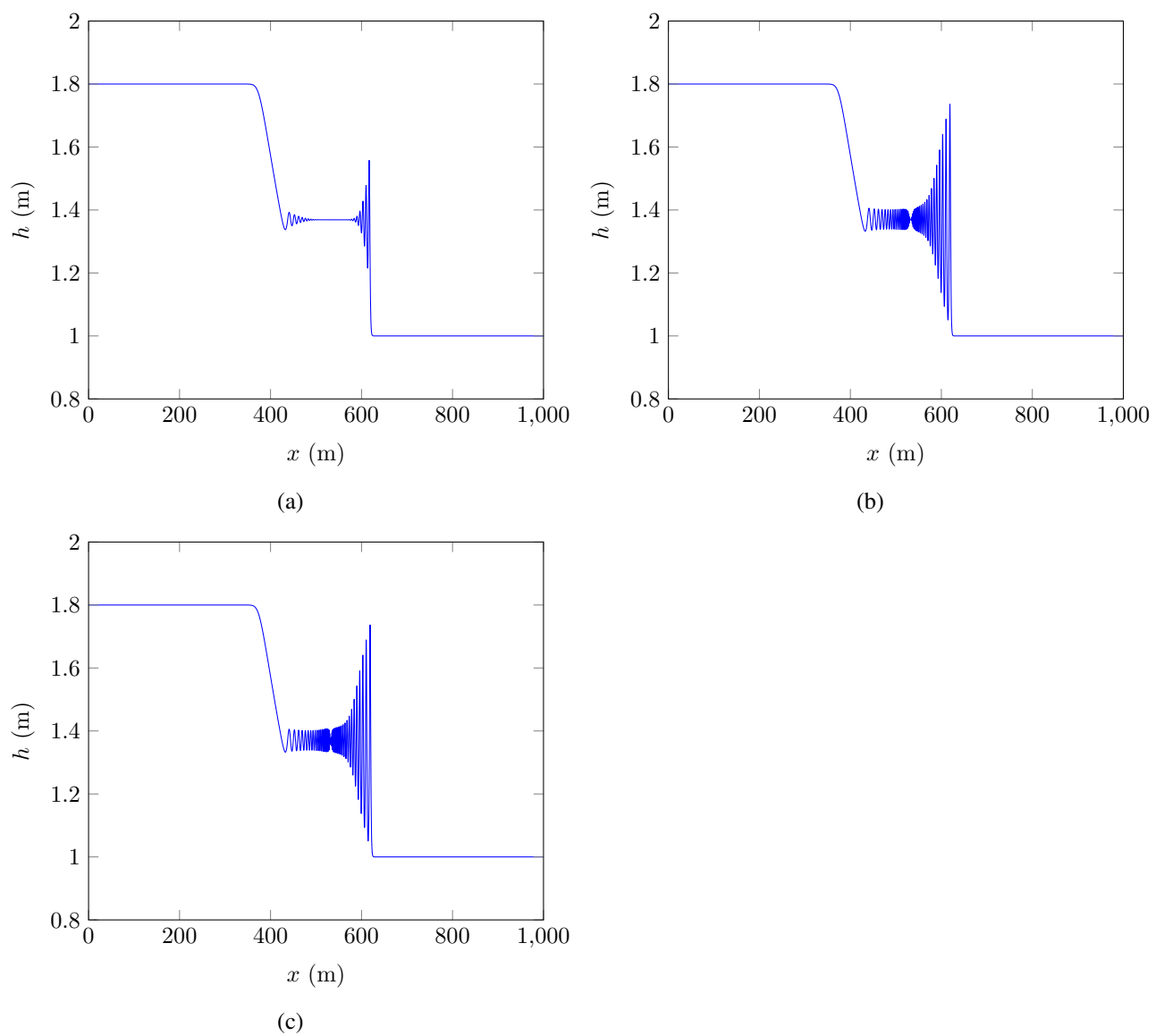


FIG. 8: Solution of the dam break problem using the (a) first-, (b) second- and (c) third-order schemes.

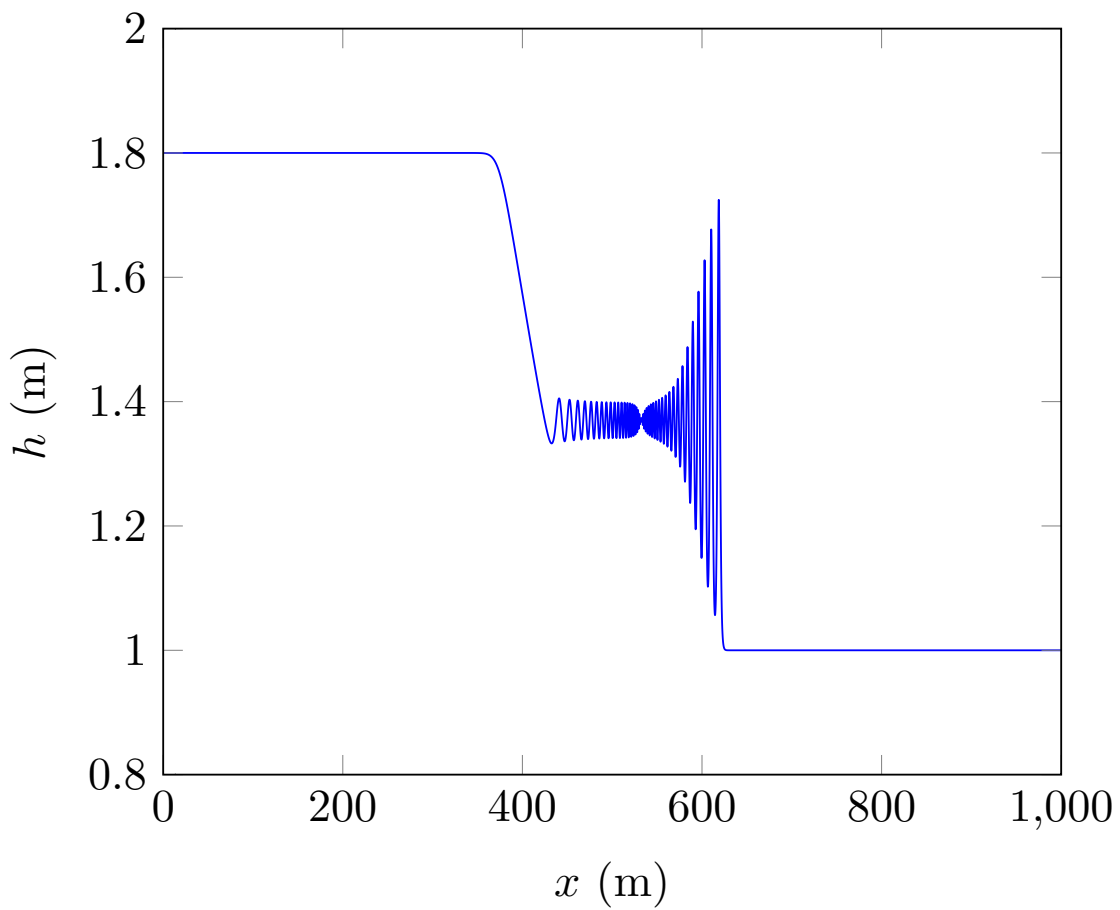


FIG. 9: Solution of the dam break problem using first-order scheme with  $\Delta x = 100/2^{16}$ m